AIMS Energy, 11(3): 404–422.
DOI: 10.3934/energy.2023021
Received: 28 November 2022
Revised: 06 April 2023
Accepted: 11 April 2023
Published: 23 April 2023

http://www.aimspress.com/journal/energy

Research article

Inertia compensation of power grid with flywheel-integrated synchronous condenser

Parveen Tania*, Sanjari Mohammad J. and Arace Luke

School of Engineering and Built Environment, Griffith University, QLD, Australia

* **Correspondence:** Email: t.parveen@griffith.edu.au; Tel: +61421767499; Fax: +61421767499.

Abstract: This paper studies the integration of flywheel energy storage system (FESS) to a synchronous condenser (SC) and its effect on the stability margin of the power system. To show the applicability of FESS-integrated SC in mitigating sudden power loss and sudden load implementation, the experimental and simulation results are presented.

Keywords: flywheel energy storage system; synchronous condenser; power system stability; induction motor

Abbreviations: PV: Photovoltaic system; SC: Synchronous condenser; SVC: Static var compensator; AEMO: Australian energy market operator; RES: Renewable energy source; FESS: Flywheel energy storage system; DACI: Data acquisition and control interface; ROCOF: Rate of change of frequency; LVDAC-EMS: Labvolt DACI energy management software; SI: Synthetic inertia; p: Number of pole pairs; S: Machine rating power (VA); H: Machine inertia constant (s); T_e: Rotor electromechanical torque (N.m); T_L: Mechanical losses (N.m); P_e: Electrical power (W); P_m: Mechanical power (W); P_D: Frequency dependent load power (W); P_{D_0}: Steady state frequency dependent Load power (W); P_{e_0}: Steady state electrical power (W); ΔP_{e_0}: Perturbation (W); ω: Angular velocity of flywheel (rad/s); ω_m: Angular mechanical velocity of flywheel (rad/s); ω_e: Angular electrical velocity of flywheel (rad/s); ω_{e_0}: Steady state angular velocity (rad/s); J_c: Inertia (kg.m^2); E: Kinetic energy (J); K_D: Damping factor (Ns/m)

1. Introduction

The operation of large-scale wind farms and centralized solar PV farms brings lack of reactive power and voltage drop issues [1]. A large share of renewable energy sources (RES) in modern grid decreases rotational inertia and leads to low system inertia compared to traditional power generation sources. This is a common experience for system operators around the world [2] and leaves the power

system's frequency vulnerable and susceptible to frequency instability [3,4]. Our electronic appliances are rated for the nominal system frequency (50 Hz), and large-scale faults cause frequency fluctuation, which was a leading factor in the South Australia blackout in 2016 [5]. The combination of system separation and frequency collapse resulted in a black system. Consequently, the Australian Energy Market Operator (AEMO) deemed it no longer appropriate to rely solely on synchronous generators to provide non-energy system services such as voltage control, frequency control, inertia, and system strength, and called for the need for a proof of concept for synchronous condensers (SC), rotating stabilizers, and flywheels [7–13].

SCs have been well documented for positive impact on voltage and reactive power control for more than 50 years [13–16]. Other devices, such as static var compensator (SVC), static synchronous compensator (STATCOM), and synthetic inertia (SI) devices are also used in the electric-power grid with varying capabilities [14, 17]. Conventional SC can be simply explained as a synchronous motor without a load or prime mover [3, 14, 17, 18]. SC operates as a large electric machine, where the field current is excited separately, allowing it to absorb or supply reactive power around the load, regulate voltage and control frequency by offsetting inertia loss [18]. SI can be used for low inertia compensation through storage devices in an attempt to guarantee optimal network security [18]. SI can be delivered through storage devices such as flywheels, superconducting magnetic storage, capacitors, batteries, or wind turbines, which have recently been investigated by implementing SI into the wind power plants [14, 19].

Research studies have been conducted to determine the optimal location for installing SC in an electric power system network [14, 15, 20]. It has been shown that when the SC is installed at the end of the electric power line, they improve voltage stability and power flow control of the power system network [15, 21]. SCs assist in short-circuit strength, provide successful dynamic voltage recovery, and improve SI [22]. Additionally, there are various indirect advantages that SCs can deliver, such as reducing losses, saving line capacity, and increasing transfer capabilities compared to capacitor banks [21].

Traditional capacitors are installed in various locations with minimum monitoring systems, and weather conditions can affect the capacitor timers. Moreover, depending on country regulations, some capacitors in the power system are switched off in summer to avoid power factor penalties. A better way of monitoring would be to install monitoring systems at locations where capacitors are installed or to install an SC device that limits the number of capacitors functioning [1].

Many generator traders have investigated replacing small generators with SCs over the use of capacitor banks to generate benefits and cost savings. The annual cost and savings in the present value ($/MVAR) outweigh the capital cost of retrofitting an existing generator with an SC, with the full cost benefits presented in Table 1 in [1].

Rotational inertia is less likely to be present in variable renewable energy sources. Research has shown that the power and energy required to provide the SI can be quantified and have an impact on the power system's recovery [3, 19]. According to [10, 23–26],the flywheel stores kinetic energy of rotation, and the stored energy depends on the moment of inertia and the rotational speed of the flywheel. Magnetic bearings are utilized to minimize friction caused by high speed, and advanced composite materials are employed to enhance the design and performance of the flywheel [27, 28]. Numerous research and simulations utilizing MATLAB have been conducted about different control models of FESS [6]. The simulation compared the 3-phase critical load voltage with and without FESS

during a balanced three-phase voltage sag and power outage [6]. Modeling and simulating FESS in power applications are novel areas that have not been extensively studied due to the unavailability of experimental data [22, 29]. A study was conducted on the combination of SC and SI to enhance frequency stability in low-inertia systems. The ZIP load model was used to determine the motor's inertia [18]. Simulation of rotational inertia was also studied and explained in [30]. The papers [8, 24] explain the online estimation of power system inertia and minimum power system inertia requirement. The experiment described in this paper involved retrofitting a Labvolt 0.2 kW synchronous generator as an SC. Round steel flywheels with varying inertia were mounted on the same shaft to provide inertia support during power failure and load interruption. To model FESS using SC and induction motors, MATLAB/Simulink software was utilized, and the simulation results were validated with the practical application setup using Labvolt equipment.

The paper is organized as follows: In Section III, we formulate the proposed method and explain the laboratory equipment. In Section IV, we provide detailed results from extensive experiments, along with MATLAB simulation results. In Section V, we discuss the experimental results, and in Section VI, we present the conclusion and future works.

2. Methodology

2.1. Experiment setup

A three-phase salient-pole synchronous machine with a power rating of 0.2 kW is installed in a Labvolt EMS module, capable of functioning as either a three-phase motor or a three-phase generator. A flywheel is mounted onto the synchronous machine's front-end shaft and secured in place using a knob. In order to model the behaviour of transmission grid (Model 3784-1A), an innovative approach for simulating buses in the power system was implemented, utilizing an induction motor as shown in Figure 1.

2.2. Solution methodology

In order to analyze the experiment, the Data Acquisition and Control Interface (DACI) Module, along with the LVDAC-EMS Program, were utilized. The Flywheel Energy Storage System (FESS) operates under three distinct conditions: charge, stand-by, and discharge. During the charging mode, energy from the power grid is stored in the flywheel. Once the flywheel has reached its rated speed, the charging current is maintained at a consistently low level to ensure that the rated speed is maintained. In the event of a power grid failure, the FESS operates as a generator, providing power to critical loads. Following the recovery of the power grid, the FESS returns to its charging mode.

The dynamic equation that describes the behavior of the flywheel coupled with the synchronous machine can be represented as follows.

$$J_c \frac{d\omega}{dt} = T_e - T_L - B\omega \tag{1}$$

In this equation, J_c represents the combined inertia of the synchronous machine rotor and the flywheel rotor. Furthermore, the inertia constant H, a characteristic of synchronous machines, is defined as the kinetic energy E stored in the rotating mass at the rated speed divided by the machine rating power S, as illustrated in Equation (2) [10].

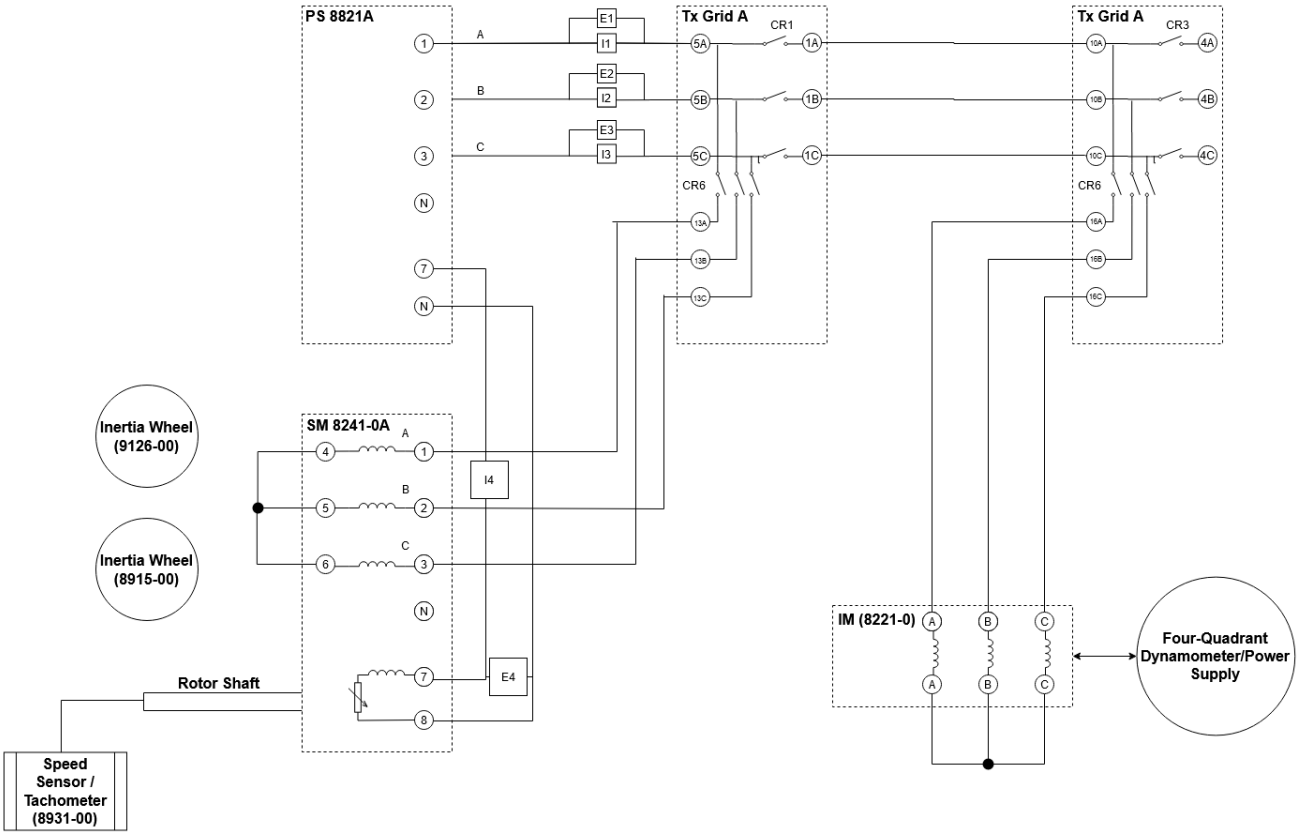

Figure 1. Experiment setup in Labvolt.

$$H = \frac{E}{S} = \frac{J\omega^2}{2S} \tag{2}$$

By having $\omega_e = p\omega_m$, and assuming $p = 1$, Eqs (1) and (2) can be reformulated as follows.

$$P_m - P_e = \omega_m \frac{2HS}{\omega_{m_0}} \frac{d\omega_m}{dt} \tag{3}$$

P_e is affected by frequency-dependent loads (PD). Assuming P_m is constant, (3) can be rewritten as follows [10].

$$P_D = P_{D_0} + K_D(\omega_e - \omega_{m_0}) \tag{4}$$

Therefore, the electric power P_e can be expressed as [10]:

$$P_e = P_{e_o} + K_D(\omega_e - \omega_{m_0}) + \Delta P_{e_0} \tag{5}$$

In steady state condition, P_m is equal to P_{e0}. The swing equation can be formulated as:

$$2H\frac{\frac{d\omega_e}{dt}}{\omega_{m_0}} = -K_D(\omega_e - \omega_{m_0}) - \Delta P_{e_0} \tag{6}$$

Therefore the solution of the differential equation is [10],

$$\omega(t) = \omega_{m_0} + (\frac{\exp\frac{-K_D t}{2HS}}{K_D} - \frac{1}{K_D})\Delta P_{e_0} \tag{7}$$

and

$$\frac{d\omega(t)}{dt} = -\omega_{m_0} + \frac{\exp\frac{-K_D\omega_{m_0}t}{2HS}\Delta P_e}{2HS} \tag{8}$$

Equation (8), the swing equation, clearly illustrates that in the event of a significant power disturbance and a system possessing a high level of inertia, the rate of change of frequency (ROCOF) would be low. As a result, power system stability can be maintained [31].
Hence, in this paper, small and large flywheels are coupled with a SC in order to assess the level of voltage support that can be offered to the power grid under two distinct scenarios:

1. Blackout period when power supply is totally turned off
2. Load disturbance when the induction motor is totally turned off

The second scenario can be further divided into four distinct cases, namely the base case, SC with field excitation, SC with small flywheel, and SC with large flywheel. To validate the experimental findings, simulations are also conducted using the MATLAB/Simulink platform.

3. Result

Experimental and simulation result are provided in this section.

3.1. Experimental result

During the experimental process, several parameters of the synchronous machine, such as voltage, active and reactive power, as well as the speed and field current, are recorded in three distinct modes of operation: charging, standby, and discharging. The experimental scenario is comprised of three modes, namely standby for 10 seconds, power shutdown for 10 seconds (resulting in the discharging of SC), and flywheel charging for 10 seconds (to achieve synchronous speed). The data collected during the experiment is measured at a rate of 1 sample per second and exported via the LVDAC-EMS program to a database for subsequent calculations and graphical representation.

3.1.1. Scenario 1: Power supply is completely turned off in SC only system

The SC successfully maintained a synchronous speed of 1500 rpm until the mode change, after which it gradually decreased to 0 rpm over a period of 8 seconds. It then returned to steady state and was able to reach synchronous speed once again after 2 seconds. When the field excitation was still connected at 20 seconds while entering the charging mode, a higher field current was observed, leading to a negative reactive power spike in Figure 3 as the motor braked. Figure 2 indicates that by 12 seconds, all values had returned to zero. The non-linear step observed at 11 seconds was attributed to the excited magnetic field of the rotor and the voltage of the stator windings.

Figure 3 shows negative values at 11 s, indicating the generation of active power (−0.126 W) and reactive power (−0.461 Var) by the synchronous motor.

SC with small flywheel: This section presents an analysis of the Labvolt 8915-flywheel model (0.028 kgm^2) coupled to the rotor of the synchronous generator.

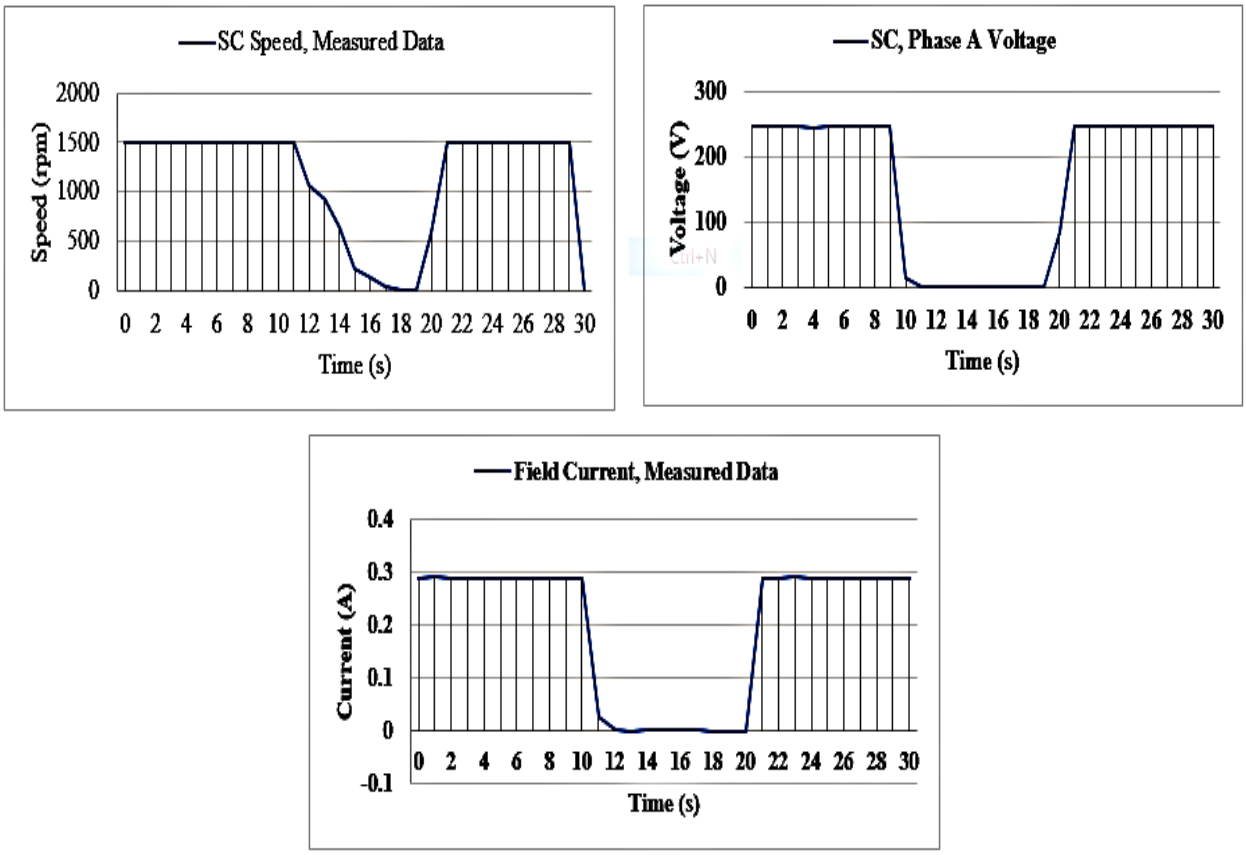

Figure 2. Speed(a), voltage(b) and field current(c) of SC during mode transition.

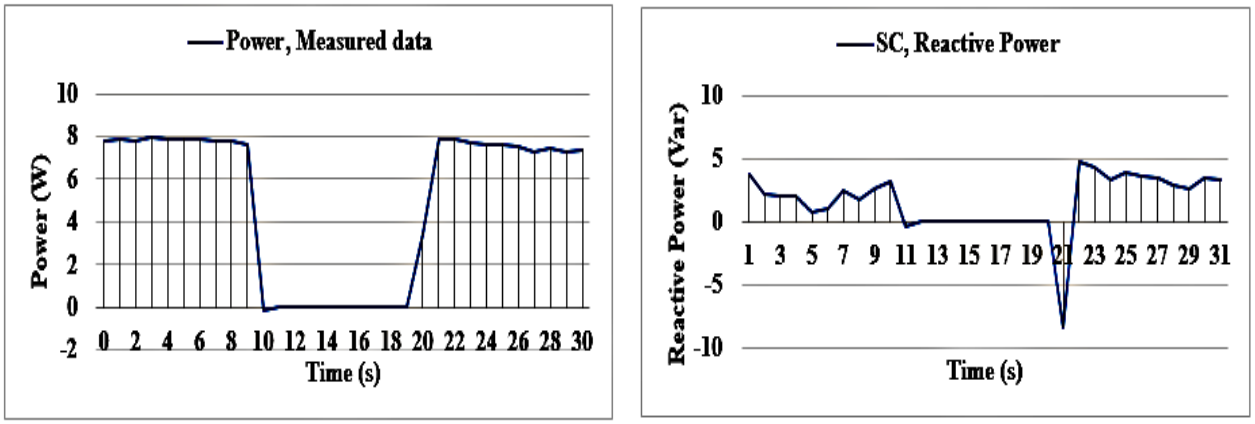

Figure 3. Real and Reactive power of SC during mode transition.

Figure 4 illustrates the synchronous speed response during the mode transition. The synchronous generator was able to maintain a synchronous speed of 1500 rpm until the mode was changed, and then decreased to 1140 rpm after 10 seconds. At t = 21 s, the speed was 1475 rpm, and at t = 22 s, it was 1510 rpm. The speed continued to oscillate and eventually reached the synchronisation speed of 1500 rpm. Additionally, the field current followed a decreasing trend in tandem with the rotor's speed until t = 16 s when the field current reached 0 A in Figure 4.

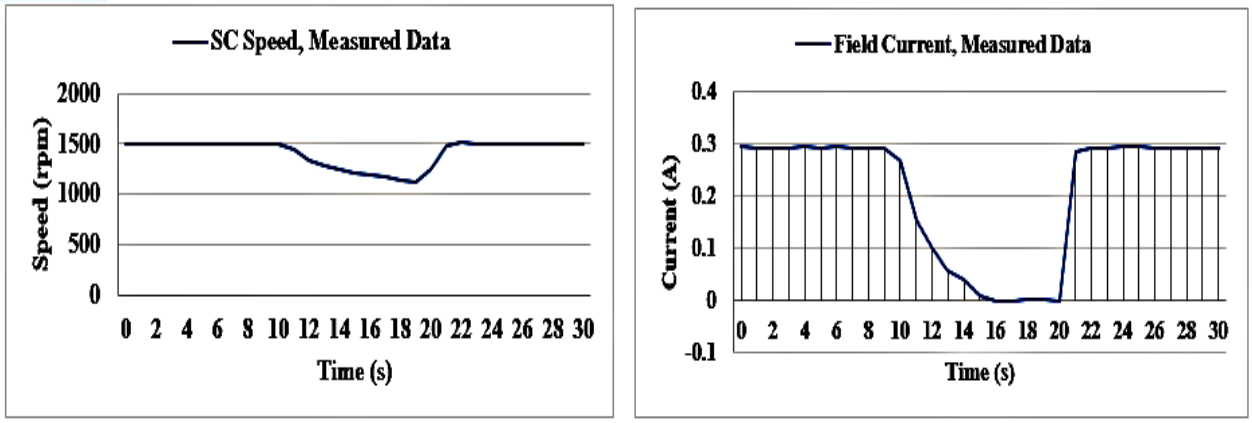

Figure 4. Speed(a) and field current(b) of SC with small flywheel during mode transition.

Figure 5 depicts the added energy to the rotor, where the active (–17.23 W) and reactive power (–12.47 Var) were measured at t = 10 s. These two parameters gradually decreased to zero at t = 16 s. At t = 22 s, a spike is observed in Figure 5, with a sudden increase in the field current, active power, and stator current. This phenomenon can be attributed to the re-synchronization of the speed, which drew more power from the grid to increase the speed. As a result, the speed increased from 1500 to 1505 rpm at that instant.

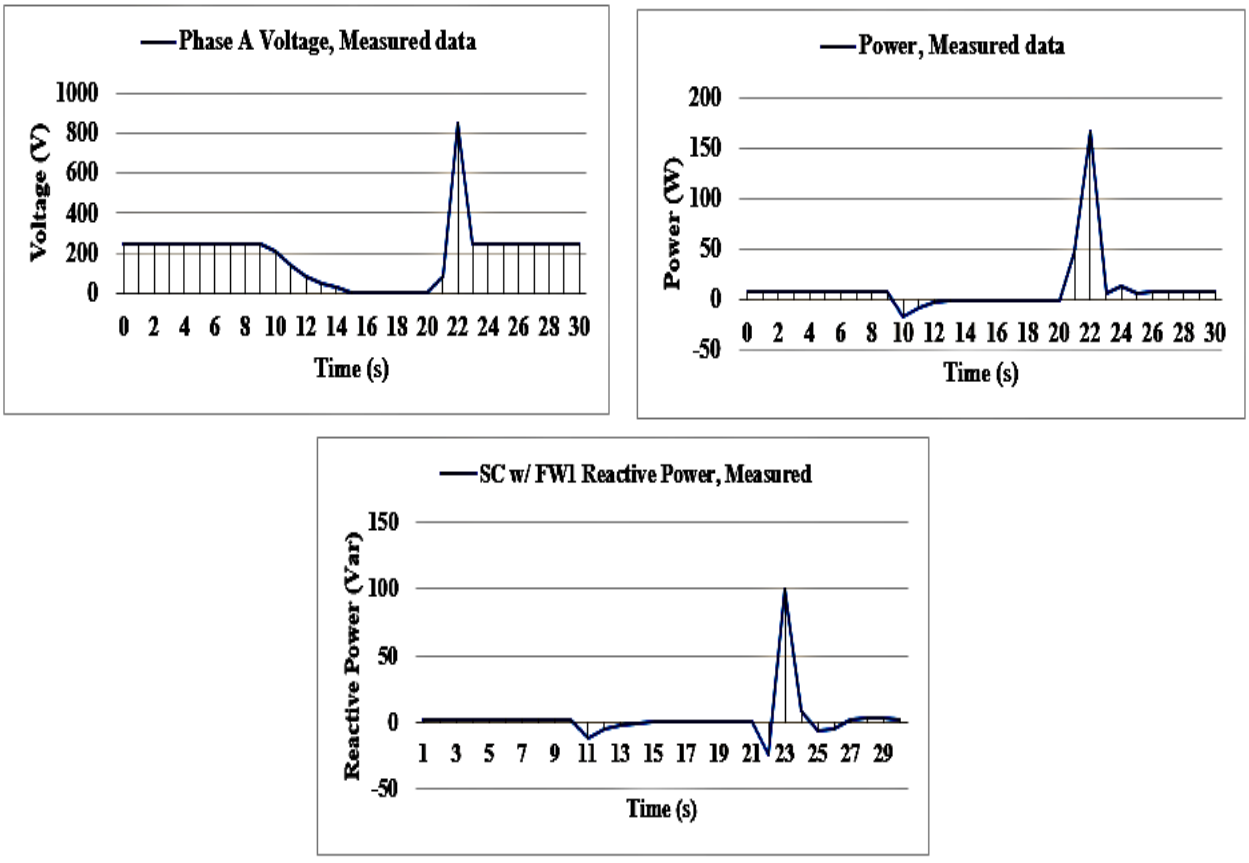

Figure 5. Speed(a), voltage(b) and field current(c) of SC during mode transition.

SC with large flywheel: An analysis of the Labvolt 9126-flywheel model (0.058 kgm^2) coupled to the rotor was conducted to assess its impact on the energy output of the SC. The findings indicated that the flywheel model added 550 J of energy to the SC at 1500 rpm. In comparison to the preceding cases, the larger flywheel was able to maintain a higher rotor speed during the discharge mode, with the speed depicted in Figure 6 reaching 1248 rpm at 19 s.

At the onset of the discharge mode, the SC generated –7.577 Var of reactive power. Contrarily, during the charging mode, which commenced at 21 s, there was no reactive power generated, in contrast to the smaller flywheel used in the previous section. The larger flywheel attached to the rotor increased the mechanical load. Nevertheless, owing to the speed of the rotor, the SC did not draw high power from the system to recharge the flywheel, drawing only 89.37 W at 22 s. As evident in Figure 7, no active power was generated in the recharge mode.

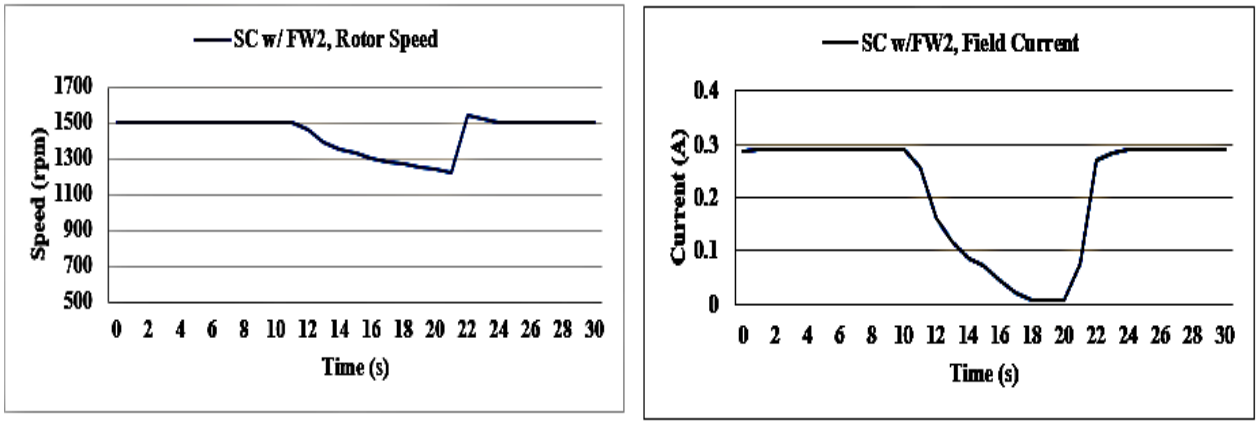

Figure 6. Speed(a) and field current(b) of SC with Large flywheel mode transition.

The additional load imposed on the rotor hindered the SC from attaining standby mode during the stipulated test period. Figure 7 portrays the rotor's speed overshooting to 1538.5 rpm, as a consequence of being in a charging state. This, in turn, led to fluctuations in SC speed and L-N voltage, in an endeavor to achieve synchronous speed of 1500 rpm.

3.1.2. Scenario 2: Load disturbance

This study investigates the contribution of flywheel coupling to the SC for frequency stability under load disturbance. The investigation is carried out in four cases: induction motor base case, SC with field excitation, and SC with field excitation and two models of flywheel, namely 8915 and 9126, to meet the standards specified by the power system operator [34]. The configured system for analysis is shown in Figure 1.

As described in scenario 1, the synchronous motor/generator was operating at synchronous speed prior to initializing the measurement, which stored maximum energy in the flywheel. In the absence of a field-oriented control system, the test was conducted over 60 seconds to enable manual increase of the field excitation voltage. Once the system was stabilized, the four-pole squirrel-cage induction motor was introduced to the system via the transmission grid switch. The power and frequency were recorded to determine the impact of load disturbance. The speed, voltage, and power factor were also measured to discuss the results in relation to other parameters.

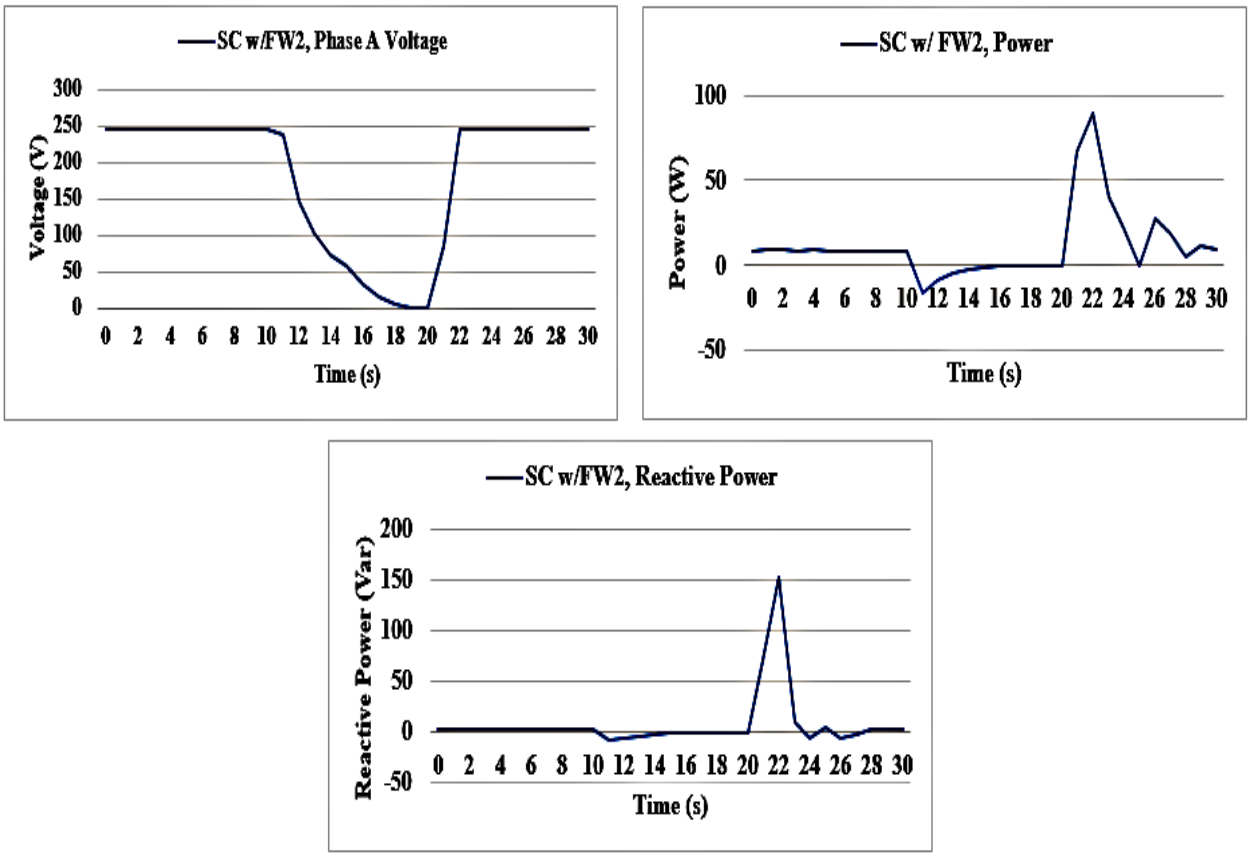

Figure 7. Voltage(a), real(b) and reactive power(c) of SC with Large flywheel mode transition.

Case 1: base sase Figure 8 shows the system frequency response, speed and power factor changes due to sudden connection of induction motor to the system.

Case 2: SC with field excitation At the condition of working SC at synchronous speed, the field excitation was increased to reduce the reactive power close to zero.

As shown in Figure 9, speed of the SC oscillated around 1500 rpm (f = 50 Hz) due to inconsistent voltage at the field due to the lack of control. Figure 9 further demonstrates the correlation between rotor speed and system frequency. An increase in field voltage caused the load disturbance of the induction motor. It can be observed from Figure 9 that during the connection of the induction motor, the frequency fluctuated until the activation of the field voltage control. As the field excitation increased, the frequency decreased, and the power in the system increased in comparison to the pre-load state.

Case 3: SC and flywheel model 8915 (0.028 kgm^2) with field excitation Case 3 is similar to Case 2, but with the addition of a flywheel coupled to the rotor of the SC. The fluctuation in speed consequently affects the frequency, thus accounting for the observed drop in frequency prior to the load disruption owing to a decline in rotor speed. The induction motor load was imposed at 10 s, and Figure 10 indicates a 0.01 Hz change in frequency.

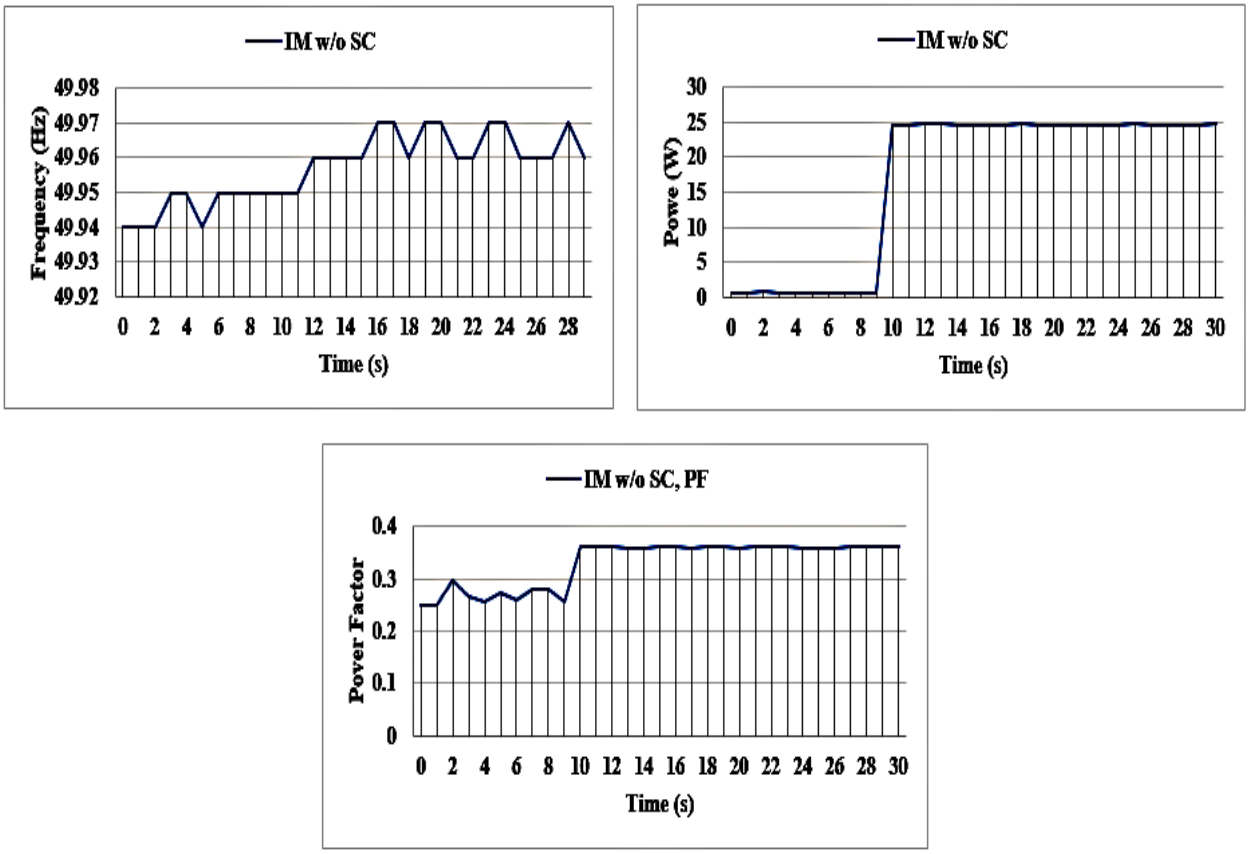

Figure 8. Frequency response, power and power factor of sudden induction motor load on stable power system.

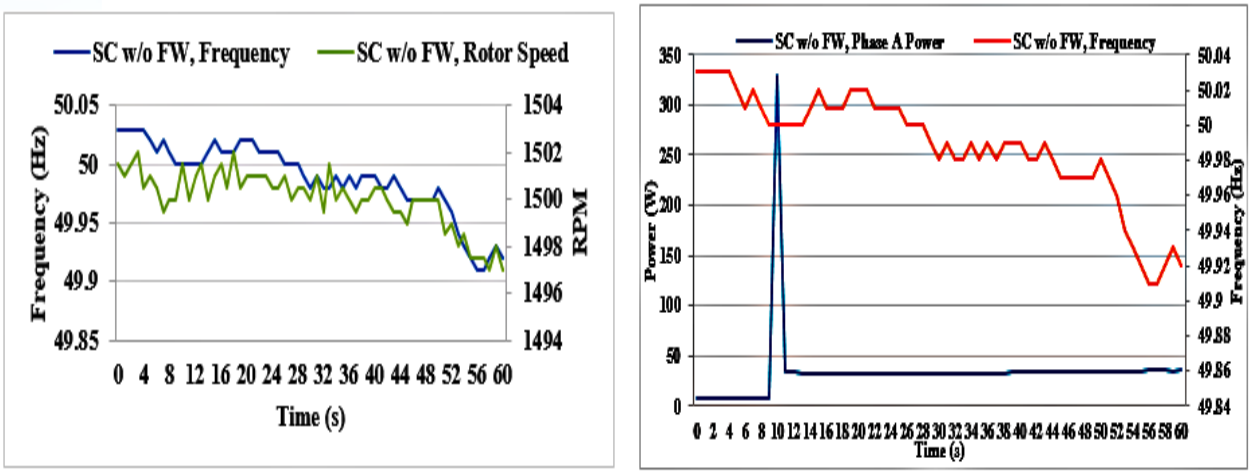

Figure 9. Speed(a) and field current(b) of SC with Large flywheel during mode transition.

Subsequent to an augmented load, the frequency remained steady, exhibiting a deviation from 49.91 Hz at 5 s to 49.88 Hz at 20 s, as displayed in Figure 10.

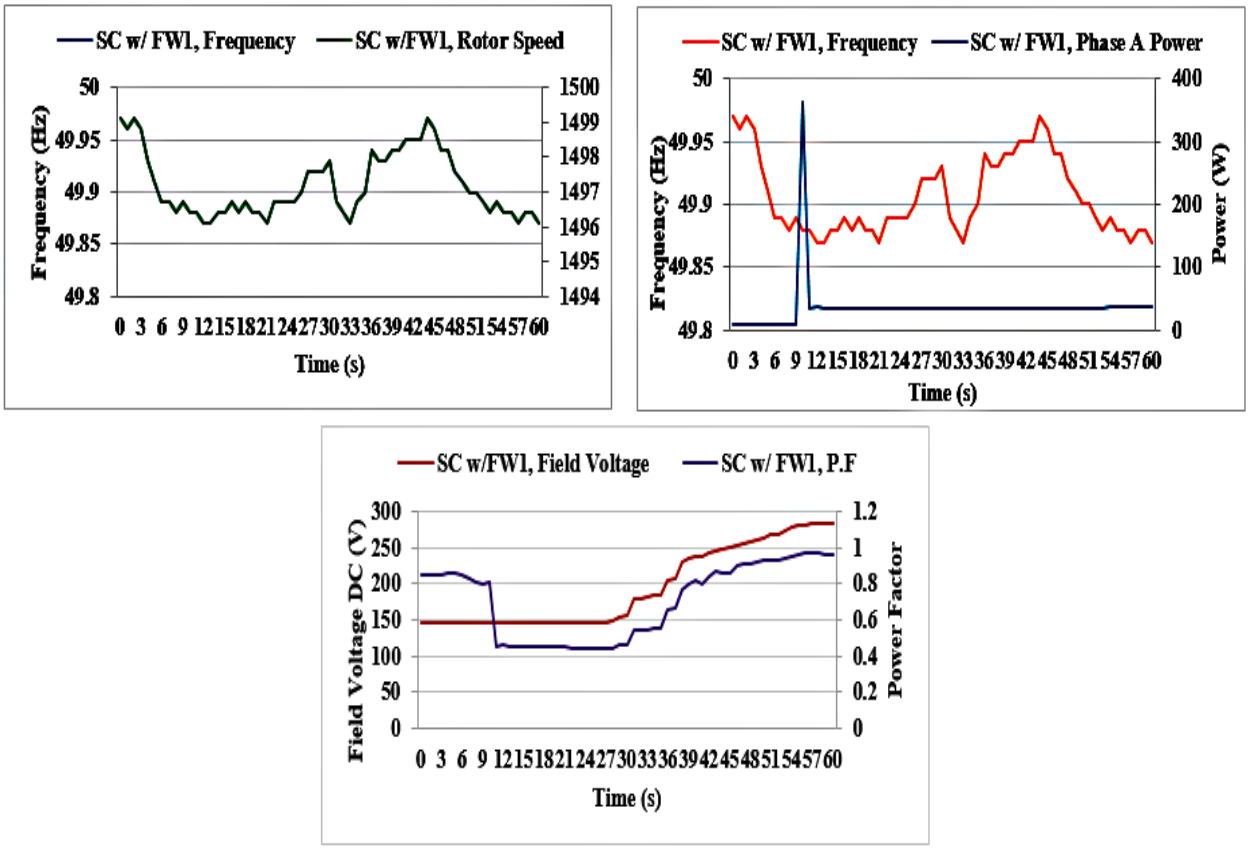

Figure 10. Voltage(a), real(b) and reactive power(c) of SC with large flywheel during mode transition.

Case 4: SC and flywheel model 9126 (0.058 kgm^2) with field excitation Case 3 was repeated with the flywheel model 9126 having an inertia of 0.058 kgm^2, coupled to the rotor of the SC. The induction motor was connected as a load disturbance at 9 s. The frequency remained stable at the time of disturbance, and only slight deviations were detected at 15 s and 16 s, as shown in Figure 11.

3.1.3. Matlab/Simulink simulation

Scenario 1: The experimental parameters used in MATLAB/Simulink were identical to those employed to set up the system depicted in Figure 1. The simulation ran for a duration of 30 s. At the power supply end, a 3-phase fault was applied, lasting for 10 s, starting at 10 s and being cleared at 20 s. The synchronous machine initiated as an induction machine and attained the rated speed of 1 pu (1500 rpm) as a synchronous motor after 3 s. Subsequently, the field voltage was modified to 1.5 pu, and the motor operated as an SC, providing reactive power to the system grid. As illustrated in Figure 12, the speed plummeted from 1500 rpm to 0 rpm, with negative speed being visible. It is imperative to note that no governor control was employed in this experiment. However, in actual power systems, a primary governor controller is typically activated within 500 ms to attempt to balance the demand and supply [31, 32].

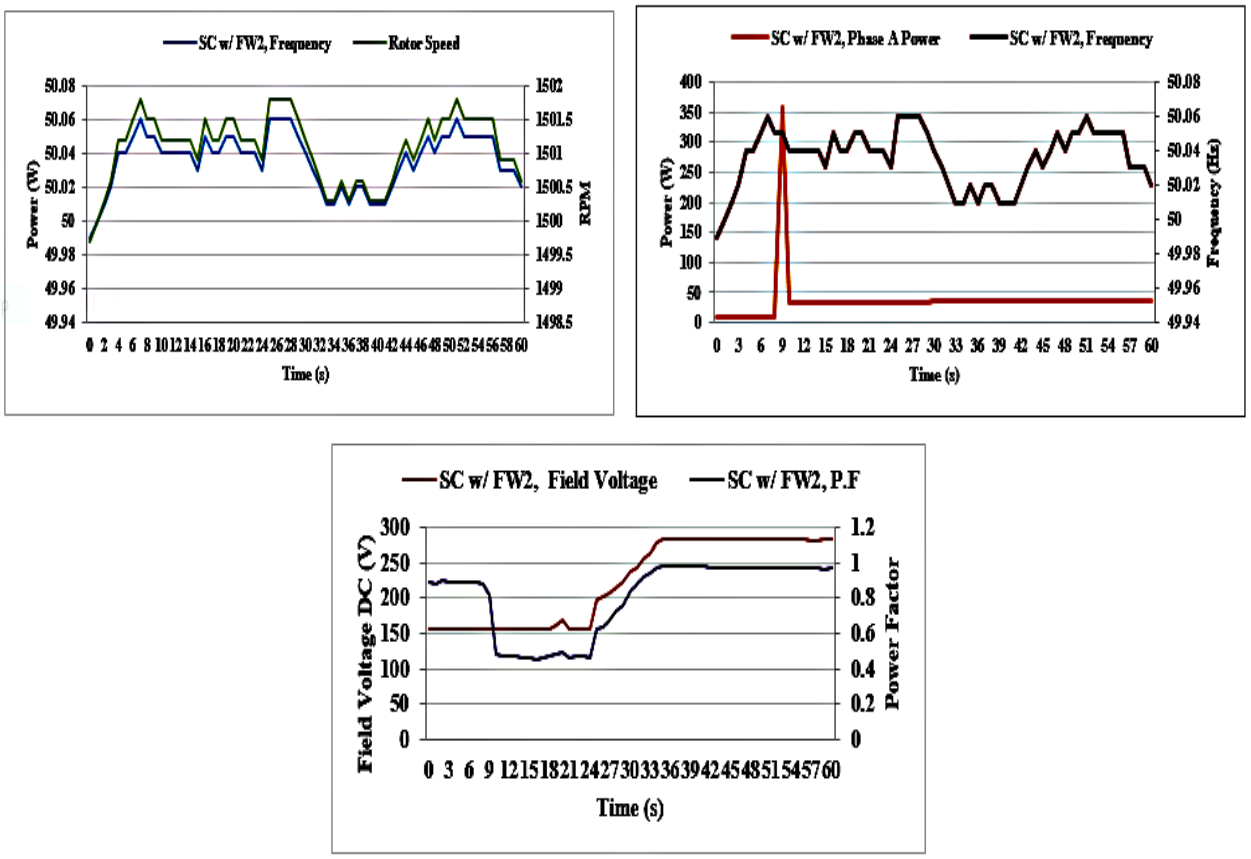

Figure 11. Voltage(a), real(b) and reactive power(c) of SC with large flywheel during mode transition.

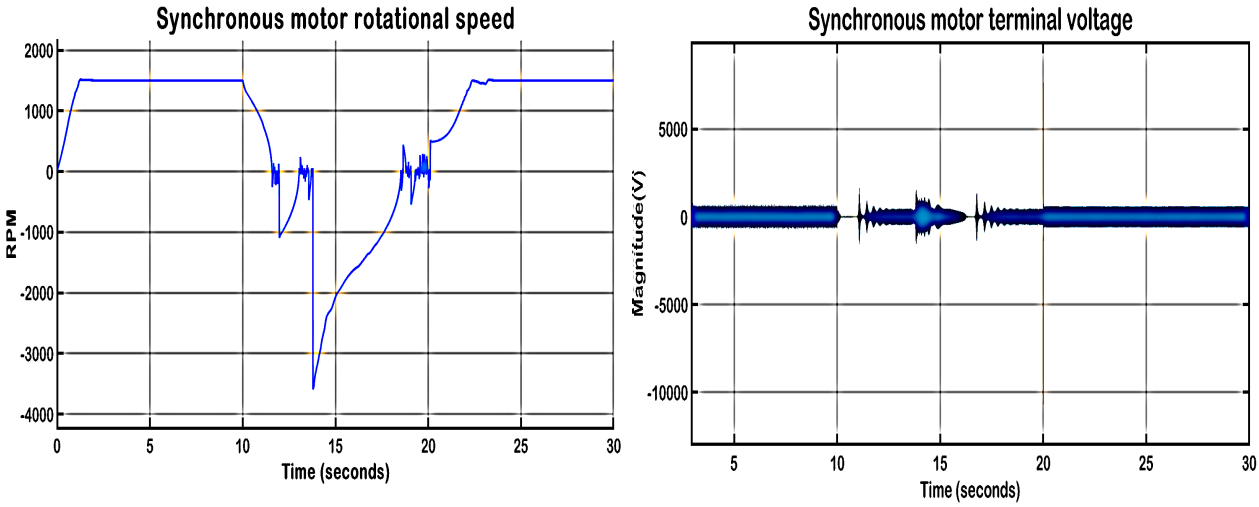

Figure 12. Speed(a) and terminal voltage(b) of synchronous machine without flywheel.

As shown in Figure 13, real and reactive power are increased when the fault happened and also when the fault cleared after 10 s.

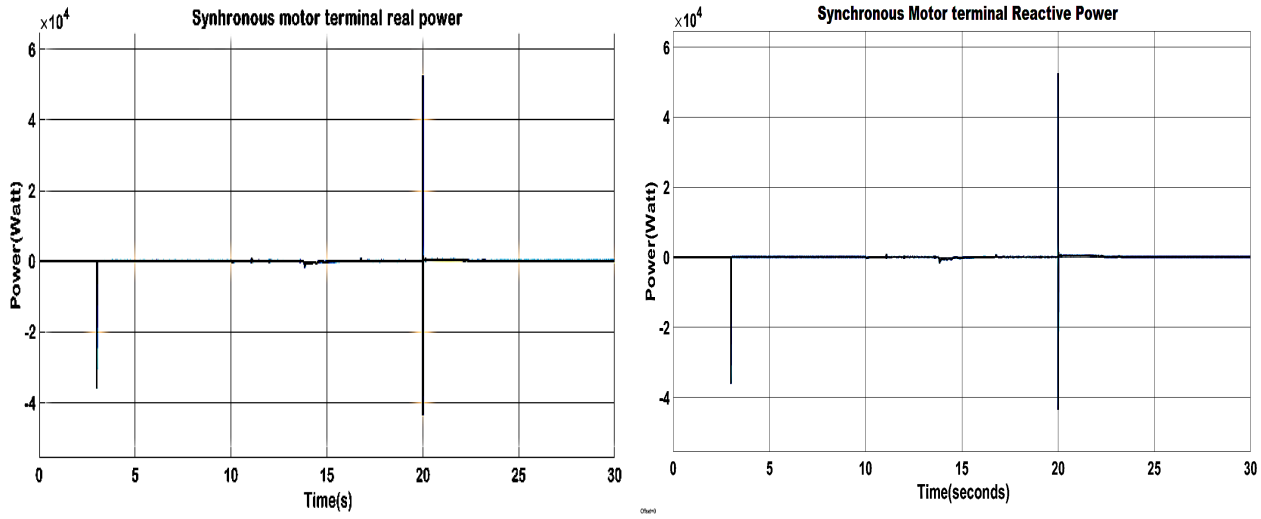

Figure 13. Real(a) and reactive power(b) of synchronous machine without flywheel.

Flywheel: Two rotational inertia blocks, i.e., 0.028 kgm^2 and 0.058 kgm^2 are emulated as small and large flywheels attached to the SC shaft with clutch in MATLAB/Simulink. The speed and voltage of SC with small flywheel are shown below in Figure 14 and it can be easily understood that compared with the Figure 12, how the flywheel inertia supports the system by maintaining the speed at the time of the fault.

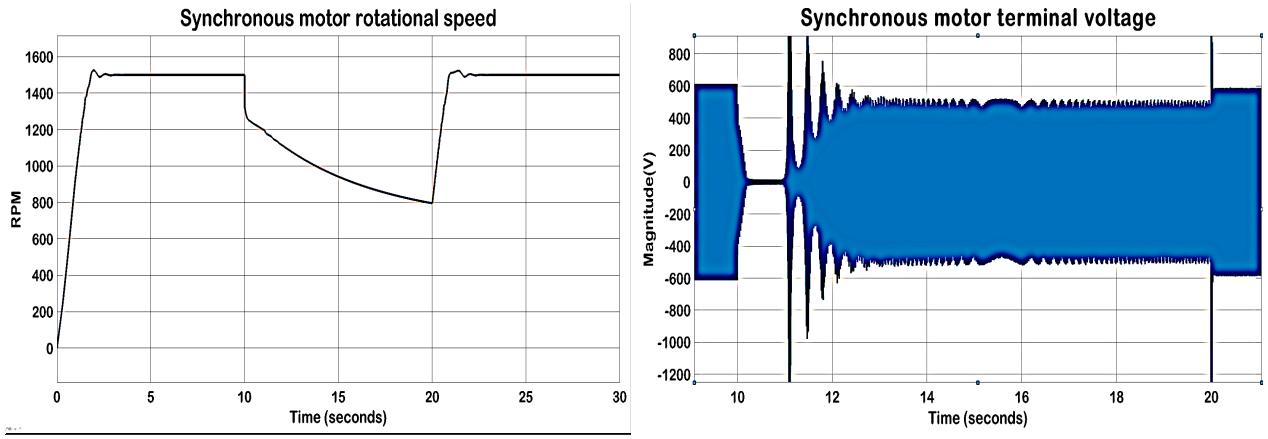

Figure 14. Speed(a) and terminal voltage(b) of synchronous machine with small flywheel.

Changes in real and reactive power during fault time are showed in Figure 15. In Figure 16(a), the system speed with the larger flywheel dropped to a greater extent at the instant of the fault compared to the scenario with the smaller flywheel. However, it also maintained a higher speed at the end of the fault compared to smaller flywheel. As shown in Figure 16(b), the system with the larger flywheel also holds a higher voltage level compared to the smaller flywheel. The real and reactive power of synchronous machine are lower in the system with the larger flywheel, as shown in the Figure 17.

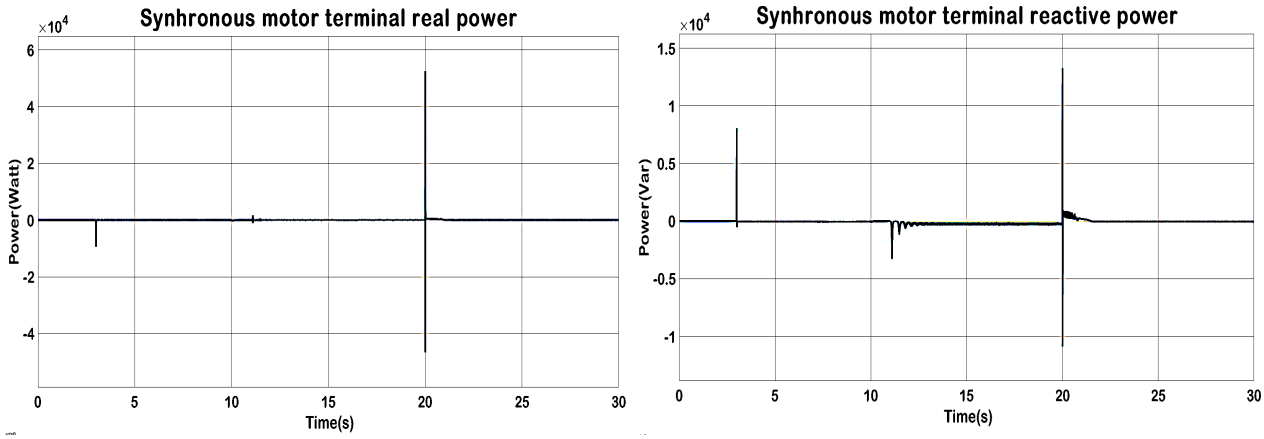

Figure 15. Real(a) and reactive Power(b) of synchronous machine with small flywheel.

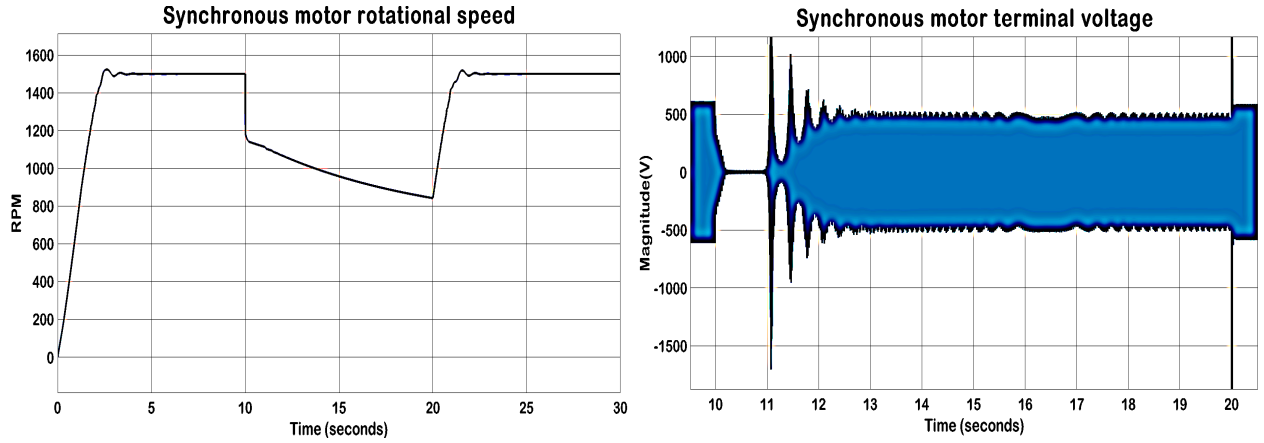

Figure 16. Speed(a) and terminal voltage(b) of synchronous machine with large flywheel.

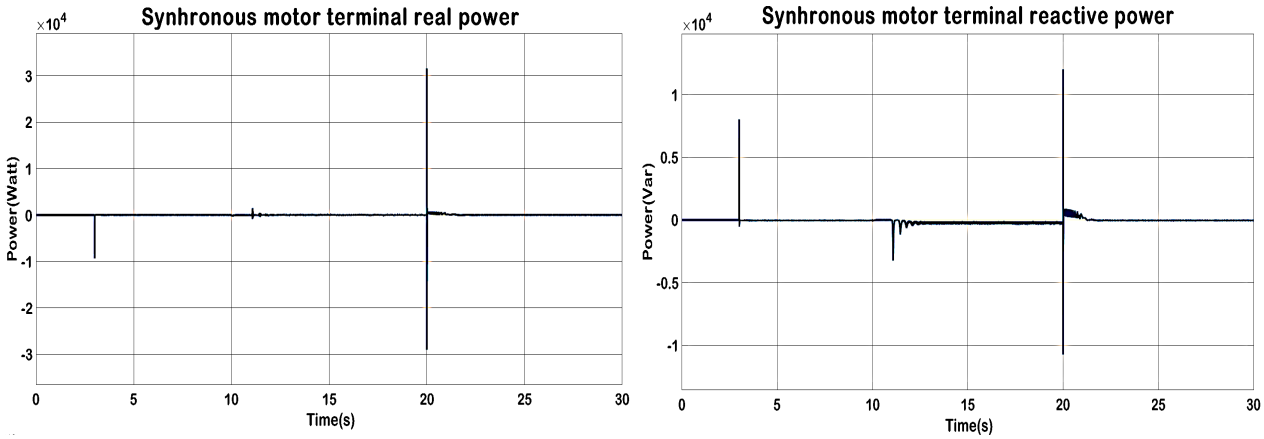

Figure 17. Real(a) and reactive power(b) of synchronous machine with large flywheel.

Scenario 2: Scenario 2 was executed using a setup similar to that of scenario 1. The synchronous motor commenced operation as an induction motor and attained a rated speed of 1500 rpm, operating as an SC after 3 s. At 10 s, an induction motor was introduced into the system. The simulation persisted for 30 s, during which the speed of the synchronous machine reduced from 1500 rpm to 1499.96 rpm.

Additionally, the power factor dropped from 0.9975 to 0.9968, lagging, and the system frequency decreased from 50 to 49.98 Hz, reaching steady-state conditions within 870.68 ms. Figure 18 presents a comparison of the speed and field current of the SC, both without a flywheel and with small and large flywheels.

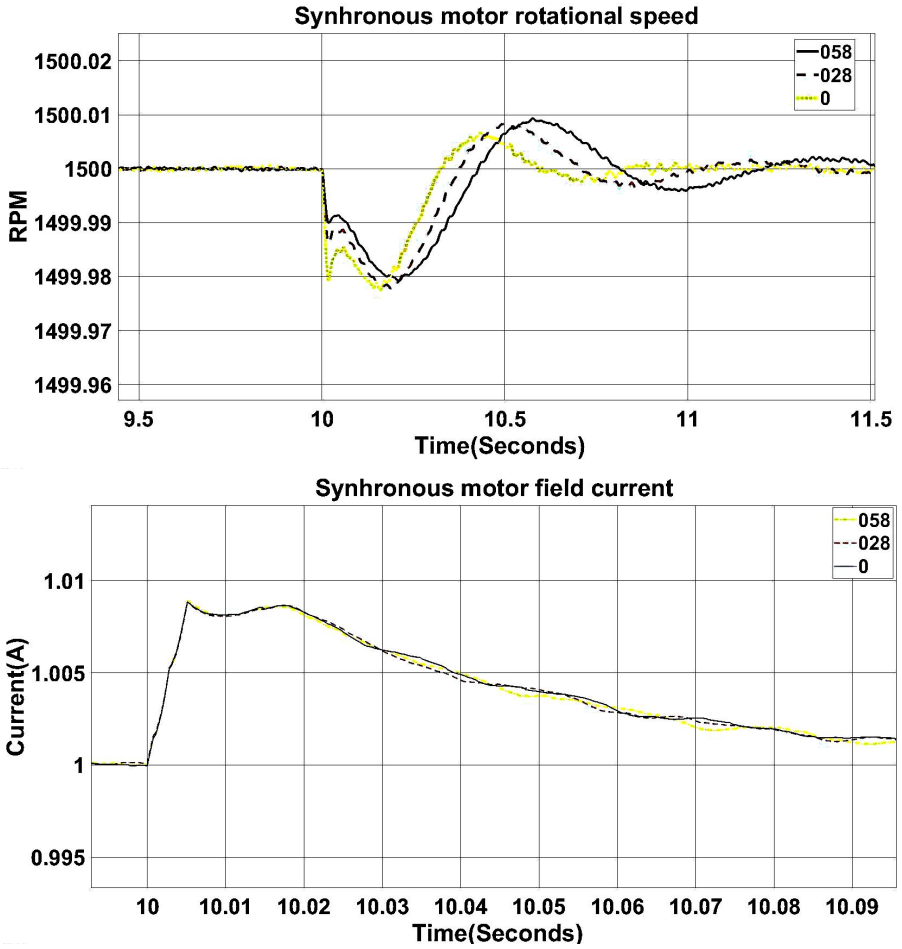

Figure 18. comparison of SC in base case, and with small and large flywheels during load disturbance: speed(a) and field current(b).

Figure 19 compares the power factor and real power of the SC with and without flywheels (small and large ones). As shown in Figure 19, during load disturbances, the power and power factor remained more stable compared to the speed depicted in Figure 18.

4. Discussion

Experimental results have successfully validated the simulations. During the experimental tests, SC parameters were measured in three different states, i.e., standby, discharging, and charging. Two different flywheels, i.e., small (0.028 kgm^2) and large (0.058 kgm^2), were compared. The use of the flywheel model during discharge allowed the system to maintain the voltage for 15 s after a complete power loss, whereas the standard SC (without any flywheel) experienced a voltage drop after only 2s.

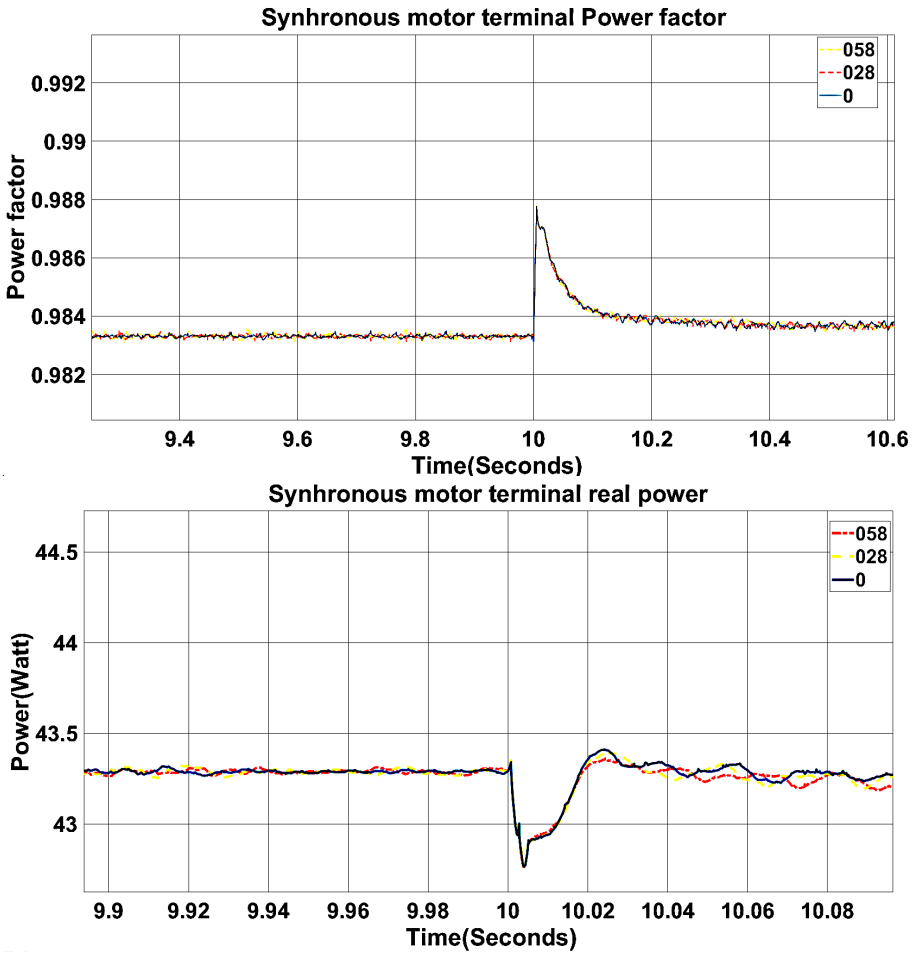

Figure 19. comparison of SC in base case, with small flywheel and large flywheel during load disturbance: power factor(a) and real power(b).

This time was extended to 19 s with a larger flywheel (0.058 kgm^2). It was observed that when the speed of SC dropped below 1290 rpm, the magnetic field of the rotor was no longer able to excite the stator windings, leading to a drop in the voltage at the terminal.

Immediately after the power loss, the standard SC was not able to operate. However, the SC coupled with the small flywheel operated between 0 and 1 s, and the SC coupled with the larger flywheel operated between 0 and 13 s due to the increased voltage and power factor required for grid destabilization. However, the SC coupled with the larger flywheel was not the most stable in the system restarting, as it was not able to reach a stable mode within the given time period.

An induction motor load was connected to investigate the frequency stability of a system using four cases. In the base case (case 1), the frequency increased by 0.03 Hz. The maximum allowed frequency deviations for contingency events are ±0.5 Hz [7]. It was observed that the coupling of the 8915 flywheel to the system (case 3) was superior, not only in terms of a higher power factor but also showing lower frequency deviation when the load disturbances occurred.

5. Conclusion and future works

The paper has successfully demonstrated the implementation of a FESS with a SC to improve grid stability. The simulation results further validate the importance of incorporating these technologies in the electric grid design to ensure a more resilient power system during power outages.

As a continuation of the proposed idea in this paper, further studies can be conducted on using a wind turbine with flywheel to enhance the grid frequency stability [34]. In-depth analysis of robustness of the FESS by reducing loss of energy during charging, stand-by and discharging is another area for future work. Research can also be conducted on reducing the time required to discharge power, minimizing disruptions in voltage and frequency, resulting in a more resilient FESS-integrated power system.

Ancklowedgement

The authors gratefully acknowledge the technical staff of Griffith University for their assistance and support during the experimental testing and preparation of this manuscript.

Conflict of interest

The authors declare no conflict of interest.

References

1. Igbinovia FO (2019) Reactive power compensation in modern electricity grid architecture with the synchronous condenser. *PhD thesis*, Czech Technical University in Prague.
2. Balint H, Istvan V, Istvan T (2019) Effect of decreasing synchronous inertia on power dynamics-overview of recent experiences and marketisation of services. *Int Trans Electr Energy Syst* 29: e12128. https://doi.org/10.1002/2050-7038.12128
3. Mustafa EA, Keith RP (2019) Combination of synchronous condenser and synthetic inertia for frequency stability enhancement in low-inertia systems. *IEEE Trans Sustainable Energy* 10: 997–1005. https://doi.org/10.1109/TSTE.2018.2856938
4. Kaushik D, Feng G, Edgar N (2020) Frequency stability of power system with large share of wind power under storm conditions. *Modern Power Syst Clean Energy*
5. AEMO. Black system in South Australia on Wednesday 28 September 2016.
6. Zhou L, Qi ZP (2019) Modeling and control of a flywheel energy storage system for uninterruptible power supply. *IEEE, 2009 International Conference on Sustainable Power Generation and Supply*. https://doi.org/10.1109/SUPERGEN.2009.5348077
7. Gu H, Yan R, Saha T (2019) Review of system strength and inertia requirements for the national electricity market of Australia. *CSEE J Power Energy Syst* 5: 295–305.
8. Gu HJ, Yanand RF, Saha T (2018) Minimum synchronous inertia requirement of renewable power systems. *IEEE Trans Power Syst* 33:1533–1543. https://doi.org/10.1109/TPWRS.2017.2720621

9. Li F, John K, Tom R (2006) A preliminary analysis of the economics of using distributed energy as a source of reactive power supply. *The U.S. Department of Energy.* https://doi.org/10.2172/930730
10. Rezkalla M, Pertl M, Marinelli M (2018) Electric power system inertia: requirements, challenges and solutions. *Electr Eng* 100: 2677–2693. https://doi.org/10.1007/s00202-018-0739-z
11. Bolund B, Bernhoff H, Leijon M (2007) Flywheel energy and power storage systems. *Renewable Sustainable Energy Rev* 11: 235–258. https://doi.org/10.1016/j.rser.2005.01.004
12. Zhang Y, Zhang X, Qian T (2020) Modeling and simulation of a passive variable inertia flywheel for diesel generators. *Energy Rep* 6: 58–68. https://doi.org/10.1016/j.egyr.2020.01.001
13. Mohanan V, Mareels MYI, Evans JR (2020) Stabilising influence of a synchronous condenser in low inertia networks. *IET Gener Transm Distrib* 14: 3582–3593. https://doi.org/10.1049/iet-gtd.2020.0178
14. Teleke S, Abdulahovic T, Thiringer T (2008) Dynamic performance comparison of synchronous condenser and SVC. *IEEE Trans Power Deliv* 23: 1606–1612. https://doi.org/10.1109/TPWRD.2007.916109
15. Igbinovia OF, Fandi G, Zden (2016) Optimal location of the synchronous condenser in electric-power system networks. 1–6. https://doi.org/10.1109/EPE.2016.7521731
16. Palone F, Gatta FM, Geri A, et al. (2019) New synchronous condenser-flywheel systems for a decarbonized sardinian power system. *IEEE Milan PowerTech* 1–6. https://doi.org/10.1109/PTC.2019.8810780
17. Liu Y, Yang S, Zhang S, et al. (2014) Comparison of synchronous condenser and STATCOM for inertial response support. *2014 IEEE Energy Conversion Congress and Exposition (ECCE), Pittsburgh, PA, USA,* 2684–2690. https://doi.org/10.1109/ECCE.2014.6953761
18. Nguyen TH, Yang G, Nielsen AH (2019) Combination of synchronous condenser and synthetic inertia for frequency stability enhancement in low-inertia systems. *IEEE Trans Sustainable Energy* 10: 997–1005. https://doi.org/10.1109/TSTE.2018.2856938
19. Saarinen L, Norrlund P, Yang W (2017) Linear synthetic inertia for improved frequency quality and reduced hydropower wear and tear. *Int J Electri Power Energy Syst* 98: 488–495. https://doi.org/10.1016/j.ijepes.2017.12.007
20. ABB Australia (2020) Synchronous condenser packages: Solving the challenges of renewable energy integration.
21. Jia J, Yang G, Nielsen AH, et al. (2017) Synchronous condenser allocation for improving system short circuit ratio. *2018 5th International Conference on Electric Power and Energy Conversion Systems (EPECS), Kitakyushu, Japan,* 1–5. https://doi.org/10.1109/EPECS.2018.8443358
22. Labvolt (2020) Available from: https://www.labvolt.com/about_us.
23. J Gonçalves de Oliveira (2011) Power control systems in a flywheel based all-electric driveline. 2011: 102. *Uppsala: Acta Universitatis Upsaliensis*. Available from: http://www.diva-portal.org/smash/record.jsf?pid=diva2%3A434755&dswid=7105.
24. Amiryar ME, Pullen KR (2017) A Review of flywheel energy storage system technologies and their applications. *Appl Sci* 7: 286. https://doi.org/10.3390/app7030286

25. Fooladivanda D, Mancini G, Garg S (2014) State of charge evolution equations for flywheels. Available from: https://arxiv.org/pdf/1411.1680.

26. Freeman E, Occello D, Barnes F (2016) Energy storage for electrical systems in the USA. *AIMS Energy* 4: 856–875. https://doi.org/10.3934/energy.2016.6.856

27. Gonzalez F, Sumper A, Bellimunt O (2012) Modeling and validation of a flywheel energy storage Lab-Setup. *IEEE PES Innovative Smart Grid Technologies Europe (ISGT Europe), Berlin*.

28. Pullen KR (2022) Flywheel energy storage. *Storing Energy (Second Edition)*, 207–242. https://doi.org/10.1016/B978-0-12-824510-1.00035-0

29. Amiryar ME, Pullen KR, Nankoo D (2018) Development of a high-fidelity model for an electrically driven energy storage flywheel suitable for small scale residential applications. *Appl Sci* 8: 1–29. https://doi.org/10.3390/app8030453

30. Ulbig A, Borsche TS, Andersson G (2014) Impact of low rotational inertia on power system stability and operation. *IFAC Proc Vol* 47: 7290–7297. https://doi.org/10.3182/20140824-6-ZA-1003.02615

31. Zeng F, Zhang J, Chen G, et al. (2020) Online estimation of power system inertia constant under normal operating conditions. *IEEE Access* 8: 101426–101436. https://doi.org/10.1109/ACCESS.2020.2997728

32. Ashton P, Saunders C, Taylor G, et al. (2015) Inertia estimation of the GB power system using synchrophasor measurements. *IEEE Trans Power Syst* 30: 701–709. https://doi.org/10.1109/TPWRS.2014.2333776

33. Taher AM, Hasanien HM, Abdel Aleem SHE, et al. (2023) Optimal model predictive control of energy storage devices for frequency stability of modern power systems. *J Energy Storage* 57: 106310. https://doi.org/10.1016/j.est.2022.106310

34. Hany HM, Tostado-Véliz M, Turky RA, et al. (2022) Hybrid adaptive controlled flywheel energy storage units for transient stability improvement of wind farms. *J Energy Storage* 54: 105262. https://doi.org/10.1016/j.est.2022.105262

AIMS Press